

Vibronic coupling in asymmetric bichromophores: Experimental investigation of diphenylmethane-d 5

Nathan R. Pillsbury, Nathanael M. Kidwell, Benjamin Nebgen, Lyudmila V. Slipchenko, Kevin O. Douglass, John R. Cable, David F. Plusquellic, and Timothy S. Zwier

Citation: *The Journal of Chemical Physics* **141**, 064316 (2014); doi: 10.1063/1.4892344

View online: <http://dx.doi.org/10.1063/1.4892344>

View Table of Contents: <http://scitation.aip.org/content/aip/journal/jcp/141/6?ver=pdfcov>

Published by the [AIP Publishing](#)

Articles you may be interested in

[Jet spectroscopy of buckybowl: Electronic and vibrational structures in the S 0 and S 1 states of triphenylene and sumanene](#)

J. Chem. Phys. **139**, 044313 (2013); 10.1063/1.4816636

[Excitonic splitting and vibronic coupling in 1,2-diphenoxyethane: Conformation-specific effects in the weak coupling limit](#)

J. Chem. Phys. **138**, 204313 (2013); 10.1063/1.4807300

[Vibronic coupling in asymmetric bichromophores: Theory and application to diphenylmethane](#)

J. Chem. Phys. **137**, 084112 (2012); 10.1063/1.4747336

[Electronic, vibrational, and rotational structures in the S 0 1 A 1 and S 1 1 A 1 states of phenanthrene](#)

J. Chem. Phys. **136**, 154301 (2012); 10.1063/1.3703755

[Decomposition of nitramine energetic materials in excited electronic states: RDX and HMX](#)

J. Chem. Phys. **122**, 244310 (2005); 10.1063/1.1929741



COMSOL
CONFERENCE
2014 BOSTON

The Multiphysics
Simulation
Event of the Year

LEARN MORE >>

COMSOL

Vibronic coupling in asymmetric bichromophores: Experimental investigation of diphenylmethane- d_5

Nathan R. Pillsbury,^{1,a)} Nathanael M. Kidwell,¹ Benjamin Nebgen,¹ Lyudmila V. Slipchenko,¹ Kevin O. Douglass,² John R. Cable,³ David F. Plusquellic,^{2,b)} and Timothy S. Zwier^{1,b)}

¹Department of Chemistry, Purdue University, West Lafayette, Indiana 47907-2084, USA

²Quantum Electronics and Photonics Division, Physical Measurement Laboratory, National Institute of Standards and Technology, Boulder, Colorado 80305-3328, USA

³Department of Chemistry and Center for Photochemical Sciences, Bowling Green State University, Bowling Green, Ohio 43403-0213, USA

(Received 11 June 2014; accepted 23 July 2014; published online 14 August 2014)

Vibrationally and rotationally resolved electronic spectra of diphenylmethane- d_5 (DPM- d_5) are reported in the isolated-molecule environment of a supersonic expansion. While small, the asymmetry induced by deuteration of one of the aromatic rings is sufficient to cause several important effects that change the principle mechanism of vibronic coupling between the close-lying S_1 and S_2 states, and spectroscopic signatures such coupling produces. The splitting between S_1 and S_2 origins is 186 cm^{-1} , about 50% greater than its value in DPM- d_0 (123 cm^{-1}), and an amount sufficient to bring the S_2 zero-point level into near-resonance with the $v = 1$ level in the S_1 state of a low-frequency phenyl flapping mode, $\nu_R = 191\text{ cm}^{-1}$. Dispersed fluorescence spectra bear clear evidence that $\Delta v(R) = 1$ Herzberg-Teller coupling dominates the near-resonant internal mixing between the S_1 and S_2 manifolds. The fluorescence into each pair of Franck-Condon active ring modes shows an asymmetry that suggests incorrectly that the S_1 and S_2 states may be electronically localized. From rotationally resolved studies, the S_0 and S_1 states have been well-fit to asymmetric rotor Hamiltonians while the S_2 state is perturbed and not fit. The transition dipole moment (TDM) orientation of the S_1 state is nearly perpendicular to the C_2 symmetry axes with 66(2)%:3(1)%:34(2)% a : b : c hybrid-type character while that of the S_2 origin contains 50(10)% a : c -type (S_1) and 50(10)% b -type (S_2) character. A model is put forward that explains qualitatively the TDM compositions and dispersed emission patterns without the need to invoke electronic localization. The experimental data discussed here serve as a foundation for a multi-mode vibronic coupling model capable of being applied to asymmetric bichromophores, as presented in the work of B. Nebgen and L. V. Slipchenko [“Vibronic coupling in asymmetric bichromophores: Theory and application to diphenylmethane- d_5 ,” J. Chem. Phys. (submitted)]. © 2014 AIP Publishing LLC. [<http://dx.doi.org/10.1063/1.4892344>]

I. INTRODUCTION

Electronic energy transfer and exciton interactions have been studied in a variety of settings in which more than one chromophore is present, including aromatic dimers¹ and bichromophoric molecules.^{2,3} Flexible bichromophores offer the opportunity to study these effects on a conformation-specific basis. Much of this work has focused attention on bichromophores in which the two chromophores are identical to one another. Among such work is a recent, detailed study of diphenylmethane ($C_6H_5CH_2C_6H_5$, DPM- d_0), using a combination of fluorescence excitation, dispersed fluorescence (DFL), and high resolution UV spectroscopy.⁴ This has led to a firm identification of both S_0 - S_1 and S_0 - S_2 origin transitions, which are separated from one another by 123 cm^{-1} . The transition dipole moment orientations obtained from the rotationally resolved UV spectra have been used to establish

the delocalized nature of the S_1 and S_2 electronic states of both DPM- d_0 and DPM- d_{12} .⁵ Single vibronic level dispersed fluorescence spectra showed striking effects of vibronic coupling associated with the intermingled vibronic levels from the two states, which produces vibronic levels with mixed S_1/S_2 character that is reflected in the emission.

This experimental work has been complemented by the development of a multi-mode vibronic coupling model general enough to handle both symmetric and asymmetric bichromophores, and to allow for the inclusion of low-frequency inter-monomer modes.⁶ In the original work, this model was applied to DPM- d_0 , a symmetric bichromophore which had significant Franck-Condon activity in low-frequency phenyl torsional and butterfly modes. The model provided a quantitatively accurate account of the intensities and frequency positions of the observed vibronic structure both in excitation and in emission, demonstrating that the reformulated model was accurate in the symmetric limit.

The present work represents an important extension of both experiment and theory to DPM- d_5 , representing a small but significant asymmetry associated with deuteration of all

^{a)}Present address: Appvion, Inc., 825 East Wisconsin Avenue, Appleton, Wisconsin 54912-0359, USA.

^{b)}Authors to whom correspondence should be addressed. Electronic addresses: david.plusquellic@nist.gov and zwier@purdue.edu

five hydrogens on one of the two aromatic rings. From an experimental viewpoint, the spectroscopy of DPM- d_5 is fascinating in that the asymmetry induced there is exclusively due to zero-point energy effects, and therefore might be anticipated to lead to minor effects. However, the anticipated magnitude of this asymmetry is a sizable fraction of the S_1 - S_2 splitting in DPM- d_0 , and therefore can induce significant differences in the nature of the vibronic coupling between the two chromophores.

Here, we once again combine vibronic level fluorescence excitation and DFL spectroscopy on DPM- d_5 with high resolution UV spectra to identify the S_0 - S_1 and S_0 - S_2 origins, and make near-complete assignments of the observed vibronic bands in the first 300 cm^{-1} of the excitation spectrum. We also examine the impact the nuclear asymmetry of DPM- d_5 has on the transition dipole moment orientations observed in the S_1 and S_2 states and discuss the implications regarding the localized versus the delocalized nature of the wave functions.

As we shall see, both the vibronic level and rotationally resolved spectra provide evidence that the S_1 origin is electronically delocalized, much as it is in DPM- d_0 , but that all transitions in the region of the (nominal) S_2 origin are electronically mixed. The $S_1(v)$ levels responsible for this mixing are identifiable from the DFL spectra, providing a detailed state-to-state characterization of the mixing. Emission into ring modes, which come in pairs that are close in frequency, are analyzed in some detail, shedding further light on the fascinating way that isotopic substitution affects the form of these modes and the emission into them.

While the present experimental study provides a qualitative understanding of the spectroscopy of DPM- d_5 , it does not include a fully descriptive theoretical model. In response to this need, Nebgen and Slipchenko have developed an asymmetric vibronic coupling model which is applied to DPM- d_5 in Ref. 7, that provides a quantitatively accurate account of the observed spectra with relatively minor adjustments to the parameters used for DPM- d_0 .

II. EXPERIMENTAL AND COMPUTATIONAL METHODS

Mass-resolved resonant two-photon ionization (R2PI) spectra were obtained in a pulsed, supersonic molecular beam using an apparatus described previously.⁸ Diphenylmethane- d_5 (DPM- d_5) was heated to 350 K and seeded into an expansion of helium at a pressure of 3.0 bars. The free jet expansion was skimmed and the resulting molecular beam was interrogated by an unfocused, frequency-doubled neodymium-doped yttrium aluminum garnet (Nd:YAG) pumped dye laser in the focal region of a linear time-of-flight mass spectrometer. Resonantly produced parent ions of mass 173 amu were monitored as function of the laser wavelength to obtain the R2PI spectra. Laser-induced fluorescence (LIF) and dispersed fluorescence (DFL) experiments were carried out in a free jet fluorescence detection vacuum chamber at Purdue which has been described previously.⁹ Briefly, DPM- d_5 was heated to approximately 340 K to achieve sufficient vapor pressure, entrained in 2.5 bars of helium, and pulsed as a supersonic expansion into a vacuum chamber. The frequency-doubled out-

put of a Nd:YAG pumped dye laser intersected the gas pulse perpendicularly in the collision free regime of the free jet expansion. LIF spectra were obtained by scanning the laser wavelength and collecting the fluorescence using a photomultiplier tube. Furthermore, DFL spectra were recorded while placing the laser wavelength on a particular vibronic band in the excitation spectrum and dispersing the emission onto a CCD camera (Andor series DU440BT). The camera was held at -80°C using thermoelectric and water cooling, and the typical resolution using a $50\text{--}100\text{ }\mu\text{m}$ entrance slit to the monochromator was $6\text{--}8\text{ cm}^{-1}$. Scattered light was also subtracted from the DFL spectra. The details of the synthetic procedure for DPM- d_5 are discussed in the supplementary material.¹⁰

Rotationally resolved fluorescence excitation spectra of DPM- d_5 were measured using a UV laser/molecular beam spectrometer described in detail in Ref. 11. Briefly, an Ar⁺-pumped (488 nm line) cw ring dye laser using Coumarin 521 generated $\approx 300\text{ mW}$ of narrow band light ($\approx 1\text{ MHz}$) near 535 nm.⁵ Approximately 1 mW of the UV light at 268 nm was generated in an external resonant cavity containing a β -barium borate crystal. DPM- d_5 was heated to 373 K in a three chamber quartz source. Typically, the vapor was mixed with $\sim 35\text{ kPa}$ (265 Torr) of Ar gas and expanded into a source chamber through a $125\text{ }\mu\text{m}$ nozzle. The molecular beam was skimmed and crossed at right angles with a slightly focused UV beam 18 cm downstream of the source. Laser induced fluorescence at the beam crossing was collected with 20% efficiency using two spherical mirrors¹² and detected using a photomultiplier and computer interfaced photon counter. The Doppler limited resolution of the spectrometer using Ar carrier gas is 18(1) MHz at 315 nm¹³ and is therefore expected to be 20(1) MHz at 268 nm. Relative frequency calibration was performed using a HeNe stabilized reference cavity¹⁴ and absolute frequencies were obtained using a wavemeter accurate to $\pm 0.02\text{ cm}^{-1}$.

Selected rotational lines of DPM- d_5 spectrum were recorded in a mini-Fourier transform microwave (MW) spectrometer¹⁵ operating between 10 and 18 GHz. Because of the small dipole moment predicted for DPM- d_5 , the MW excitation circuit was modified to include a pre-amplifier and 1 W power amplifier followed by a pin diode MW switch. Optimal excitation was achieved using $\sim 25\text{ mW}$ of MW power and a $2\text{ }\mu\text{s}$ polarizing pulse. Samples of DPM- d_5 were loaded into a heated reservoir nozzle and heated to 433 K.

Electronic structure calculations were carried out using the Gaussian 09 suite of programs.¹⁶ Geometry optimization and normal mode frequency calculations for the ground state at the B3LYP/cc-pVTZ level of theory were used to analyze the vibrationally resolved experimental data. Rotationally resolved spectra were fit to an asymmetric rotor Hamiltonian using the genetic algorithm¹⁷ as implemented in the *JB95* spectral fitting program.^{18,19} Optimized structures at the MP2/cc-pVTZ level of theory were used as input for fitting the rotational spectra.

DPM- d_5 was prepared by reduction of diphenylmethanol- d_5 (benzhydrol- d_5) using the hypophosphorous acid-iodine system as detailed by Gordon and Fry.²⁰ Diphenylmethanol- d_5 was obtained by reacting the Grignard

reagent of bromobenzene- d_5 with benzaldehyde in diethyl ether.

III. RESULTS AND ANALYSIS

A. LIF excitation spectrum

The first 1300 cm^{-1} of the R2PI excitation spectrum of DPM- d_5 is shown in Figure 1. The spectrum is dominated by a strong S_0 - S_1 origin band at 37365 cm^{-1} . S_1 ring mode fundamentals typical of a π - π^* excitation are found 540 and 925 cm^{-1} above the origin, and are closely analogous to the $6b_1^0$ and 12^1_0 modes, respectively, of toluene.²¹ A closer view of the low-frequency portion of the LIF spectrum is shown in Figure 2, containing transitions mainly due to inter-ring torsional (symmetric T and antisymmetric \bar{T}) and butterfly (β) modes. The assignments given in Figure 2 are based on DFL spectra presented in Sec. III C. We refer to these assignments in what follows as a way of introducing the key aspects of the LIF excitation spectrum.

Figure 3 depicts the form of the low-frequency inter-ring vibrations relevant to the present study. According to the calculations, these normal modes are virtually unchanged from those in DPM- d_0 , involving equal-amplitude motions of both rings. In DPM- d_0 , where the molecule retains C_2 symmetry in both S_0 and S_1 states, the symmetric torsion T has an allowed fundamental, while the antisymmetric torsion \bar{T} appears only as even overtones.⁴ In DPM- d_5 , we see a pair of transitions with nearly equal intensity, appearing at frequencies anticipated for the \bar{T} and T fundamentals. As we shall see, the progression bearing a 20 cm^{-1} spacing is ascribed to the \bar{T} mode, while the 24 cm^{-1} progression is assigned to the T mode. Furthermore, the butterfly mode fundamental, β^1_0 , is assigned to the 56 cm^{-1} peak, at a frequency similar to that in DPM.

Perhaps, the most intriguing aspects of the LIF spectrum of DPM- d_5 are the features that are different from DPM. As just mentioned, the \bar{T} fundamental is observable in the excitation spectrum and its large intensity is striking, given the seemingly minor perturbation of deuteration of one of the rings, a point to which we will return. Additionally, the group of unusually strong vibronic transitions appearing near 180 cm^{-1} is well-shifted from the transitions near 120 cm^{-1} in the

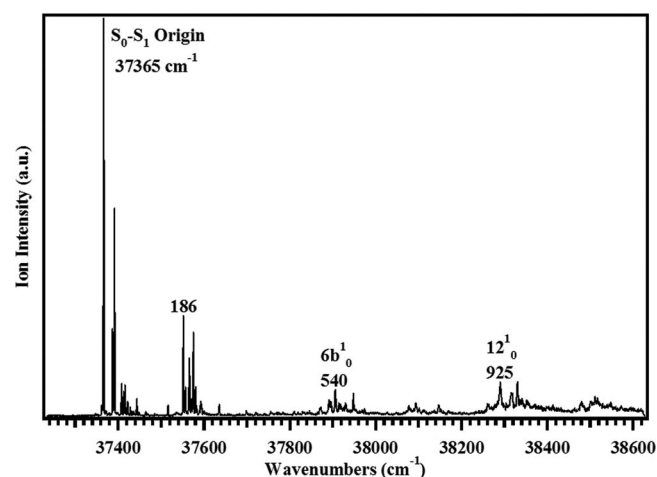


FIG. 1. Overview of the R2PI spectrum of DPM- d_5 .

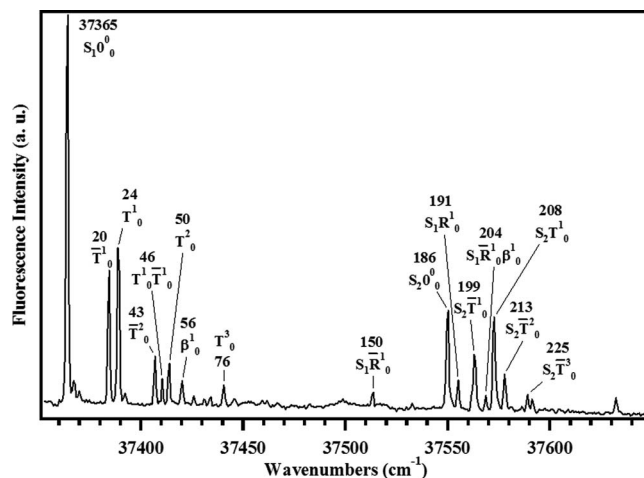


FIG. 2. Close view of the LIF spectrum. Prominent peaks are assigned and frequencies are given in wavenumbers relative to the S_1 origin.

spectrum of DPM assigned to the S_0 - S_2 origin and vibronic states mixed with it.^{4,5} On this basis, we make a first tentative assignment of the 186 cm^{-1} band in Figure 2 as a likely candidate for the S_0 - S_2 origin, and built off of it is Franck-Condon activity involving the same torsional and butterfly vibrational modes as are present in S_1 . Finally, as we shall see, unique to the LIF spectrum of DPM- d_5 are transitions that will be assigned to the symmetric and antisymmetric phenyl ring flap modes R and \bar{R} , respectively, now appearing in close proximity to the S_2 origin.

B. Rotationally resolved spectra

1. Ground state microwave spectrum of DPM- d_5

Estimates of the ground state MW transitions of DPM- d_5 were obtained from predictions using the optimized MP2/cc-pVTZ structure after hydrogen substitution with deuterium on

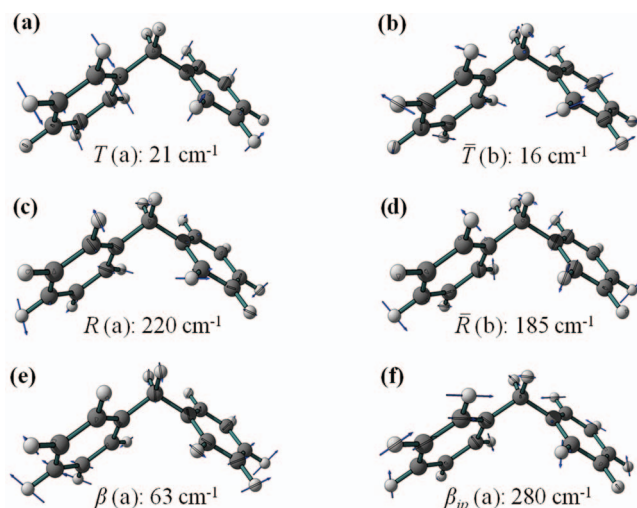


FIG. 3. Low-frequency vibrational modes calculated at the B3LYP/cc-pVTZ level of theory for the (a) symmetric torsion T , (b) antisymmetric torsion \bar{T} , (c) symmetric phenyl flap R , (d) antisymmetric phenyl flap \bar{R} , (e) butterfly β , and (f) in-plane bending β_{ip} modes. The calculated frequencies and symmetries for the C_2 point group are shown for their respective vibrations.

TABLE I. Rotational constants from least squares fits of the ground state microwave spectrum, and rotationally resolved S_0 - S_1 and S_0 - S_2 spectra of DPM- d_5 . A full list of parameters from the fits are given in Table S1 of the supplementary material.¹⁰ The squared TDM components (*a*-type, etc.) are given in percent.

Parameter	S_0	S_1	S_2	$S_1 + T^1_0$	$S_1 + \bar{T}^1_0$
$A''/\Delta A$ (MHz)	1884.0205(8)	-1.509(3)	+1.0(10)	-2.463(12)	-9.810(8)
$B''/\Delta B$ (MHz)	404.6237(6)	-1.367(2)	-2.5(10)	-1.399(1)	-1.461(3)
$C''/\Delta C$ (MHz)	399.4791(4)	-4.280(2)	-4.6(10)	-2.422(2)	-4.525(1)
$\Delta I''/\Delta \Delta I$ (u \AA^2)	-252.160(2)	9.26(1)	7.1(30)	3.03(1)	8.586(3)
<i>a</i> -type (%)	0	66(2)	30(10)	63(2)	57(4)
<i>b</i> -type (%)	60(10)	3(1)	50(10)	3(1)	7(2)
<i>c</i> -type (%)	40(10)	31(2)	20(10)	34(2)	36(4)
Origin (cm^{-1})	0	37363.94(2)	$S_1 + 185.70(5)$	$S_1 + 25.38(2)$	$S_1 + 20.79(2)$

one of the two rings and diagonalization of the moment of inertia tensor. The dipole moment of DPM- d_5 is expected to be mostly along the nominal C_2 symmetry axis, as in the parent,⁵ and therefore, spectral searches first began with low J , K_a *b*-type MW transition frequencies. These transitions were located without the need for a survey scan. Single 1 MHz sections of the spectrum were recorded and simultaneously fit to refine the predictions for higher J , K_a transitions. This procedure was repeated until all five of the first-order Watson distortion parameters were reliably fit. The inertial asymmetry also permitted the observation of a few *c*-type lines. The important rotational parameters from the linear least squares analysis of 40 *b*-type and *c*-type transitions are given in Table I. The complete set of fitted parameters and uncertainties is included in Table S1, while the list of transitions used in the fits is given in Table S2 of the supplementary material.¹⁰ Because of the inertial frame asymmetry, the distortion parameters of the Hamiltonian were those of the asymmetric re-

duction in contrast to use of the symmetric reduction in DPM- d_0 and DPM- d_{12} .⁵ The standard deviation of the line set of DPM- d_5 increased from 3.5 kHz to more than 200 kHz when the symmetric reduction was used.

2. Rotationally resolved S_0 - S_1 spectra of DPM- d_5

The rotationally resolved spectrum of the S_0 - S_1 band origin of DPM- d_5 at 267.6 nm ($37\,363.94\text{ cm}^{-1}$) is shown in panel (a) of Figure 4. The origin is blueshifted by only 42 cm^{-1} relative to the S_1 state of DPM- d_0 in contrast to the much larger blueshift of 185 cm^{-1} for DPM- d_{12} .^{4,5} Despite the inertial asymmetry, the overall spectrum of DPM- d_5 looks remarkably similar to that of DPM- d_0 , having the overall appearance of an *a*-type band because of the central Q-branch pile-up near the band origin. Given this similarity, estimates of key excited state parameters such as band type and parameter changes were based on those of DPM- d_0 . With the

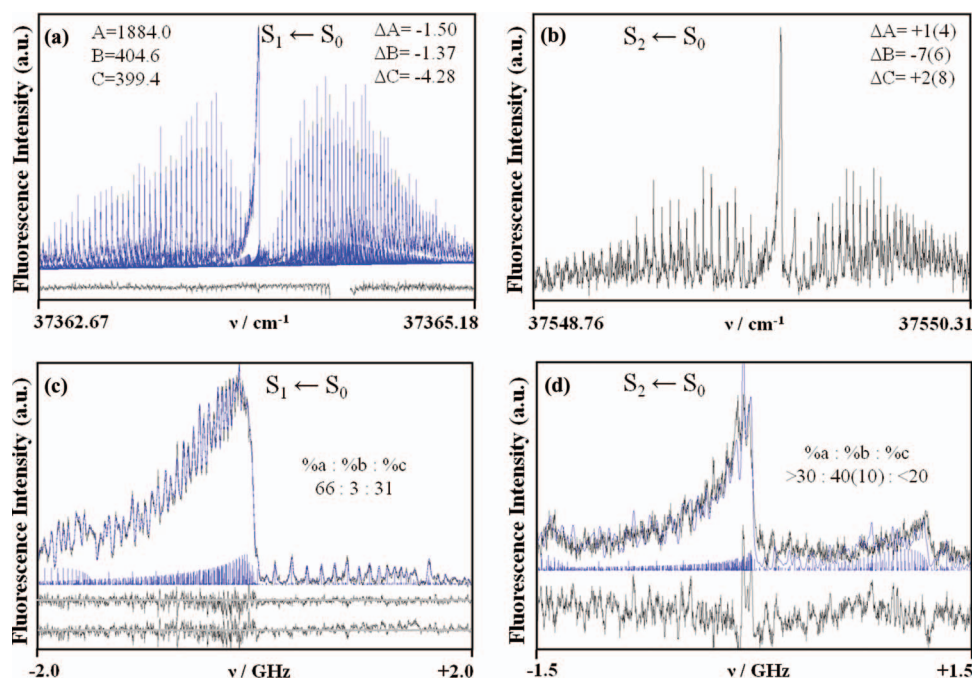


FIG. 4. Rotationally resolved spectra of the (a) S_0 - S_1 and (b) S_0 - S_2 origins and expanded portions near the band center are shown in (c) and (d), respectively. The simulated spectra are superimposed and the residuals are shown below the spectra in (a), (c), and (d). The S_0 - S_1 spectrum is well fit and the best fit parameters are shown as insets (in MHz and rounded for clarity—see Table S1 of the supplementary material¹⁰ for the fitted parameters). The S_0 - S_2 origin is poorly fit (simulated spectrum is shown in (d)) and the parameter changes relative to S_0 are only approximated. Estimates of the squared TDM components (as %) are given in (c) and (d) as insets. The lower trace in (c) shows the change in the residuals upon setting the *b*-type component to zero. The residuals in (d) illustrate the poor quality of the S_0 - S_2 origin fit. The estimated parameter ranges given in (b) and (d) are based on a set of GA runs (see text for details).

ground state constants fixed at the MW values, these estimates were included in a distributed parallel version of the Genetic Algorithm program (GA) used for the computer assisted fitting of rotationally resolved spectra.^{17,18} After only a few trial runs, the GA rapidly converged on the optimized parameters. Once the rotational constants were well determined, the hybrid band character was then fit to determine the orientation of the transition dipole moment (TDM). Since the molecular symmetry group is reduced to C_1 for DPM- d_5 , all three of the principle axes components were allowed to vary.

The residuals from the best fit simulated spectra are shown below the experimental data in panel (a) of Figure 4. The final parameters and uncertainties (type A, $k = 1$ or 1 std. dev.²²) were obtained using the traditional line assignment/linear least squares approach. A summary of the important parameters is given in Table I and a complete listing of the fitted parameters is given in Table S1 in the supplementary material.¹⁰ The changes in the rotational constants are small and similar to the small changes found in DPM- d_0 and DPM- d_{12} . The hybrid band character of the S_0 - S_1 transition is also similar: the $a:b:c$ -type band components of DPM- d_5 , specified as the squared TDM components normalized to 100%, are 66%:3%:31%, compared to the ratio of 65%:0%:35% found for DPM- d_0 . The principal difference is the small b -type component (3%) observed in the DPM- d_5 spectrum. While this component is small, it is well fit in the data as seen in panel (c) of Figure 4 from comparison of the two sets of residuals, as shown below an expanded portion of spectrum near the origin. When the b -type component is removed, the lower set of residuals shows clear deviations from the flat residuals observed when the 3% b -type character is included. The rotationally resolved spectra of the S_0 - S_1 T_0^1 and S_0 - S_1 \bar{T}_0^1 vibronic bands of DPM- d_5 are given in Figures S1 and S2 of the supplementary material,¹⁰ respectively.

3. Rotationally resolved S_0 - S_2 spectra of DPM- d_5

The rotationally resolved spectrum of the S_0 - S_2 band origin of DPM- d_5 at 266.3 nm ($37\,549.64\text{ cm}^{-1}$) is shown in panel (b) of Figure 4. The S_1/S_2 exciton splitting of 186 cm^{-1} is significantly larger than the 123 cm^{-1} and 116 cm^{-1} splittings observed for DPM- d_0 and DPM- d_{12} , respectively.^{4,5} More importantly, the overall appearance is vastly different from the pure b -type spectra observed for the S_2 states of DPM- d_0 , DPM- d_{12} and the two conformers of bis-(4-hydroxyphenyl)methane (*b4HPM*).²³ Like the S_1 origin of DPM- d_5 , the S_2 origin gives the appearance of a central a -type Q-branch.

Despite numerous attempts using a wide variety of parameter ranges in the GA, no fully satisfactory fit of the S_2 origin was possible. The simulated spectrum obtained from the average of 10 independent GA runs is overlaid with the S_2 origin spectrum in panel (b) of Figure 4. The overall rotational structure is captured in this simulation including the positions and shading of the central a -type Q-branch and b -type band heads. However, from the expanded view of the residuals shown in panel (d) of Figure 4, the detailed positions and intensities of the rotational lines are not well-reproduced. The

parameters used to generate the simulated spectrum are given in Table I. The parameter uncertainties were estimated from the ranges of the converged values obtained in the 10 independent GA runs (standard deviations are type B, $k = 1$ or 1 std. dev.²²). These uncertainties were visually confirmed by using features of the *JB95* software that permitted real time changes to the simulation and residuals upon variation of the parameters.

Despite the larger uncertainties relative to those of the S_1 state, the changes in the rotational constants in the S_2 state of DPM- d_5 are small and similar in magnitude to the S_1 state. However, in contrast to the S_2 states of DPM- d_0 , DPM- d_{12} , and *b4HPM* where pure b -type bands were observed, the squared TDM components of the S_2 state of DPM- d_5 retain only 50% of this character. Even though a small amount of mixed state character would be expected from the nuclear asymmetry as seen in the TDM composition of S_1 origin, a composition of 50% $a:c$ -type character seems well in excess of any effect from inertial frame rotation. Therefore, based on the TDM composition of the transitions assigned to the S_1 and S_2 origins, we surmise that the electronic excitation is delocalized over the two rings in the S_1 origin, much as in DPM- d_0 . However, in the transition assigned to the nominal S_2 origin, the pronounced a -type character is signaling some mixing of the S_2 origin with S_1 vibronic level(s). We turn now to DFL spectra to learn more about this mixing.

C. Dispersed fluorescence spectra

1. S_1 origin and vibronic transitions

As shown in Figure 5(a), the DFL spectrum of the S_1 origin is much like that in DPM- d_0 , with emission dominated by emission back to the ground state zero-point level, with several low-frequency transitions built off it. Emission involving the ring modes is labeled in Figure 5 using Varsanyi notation. These ring modes come in pairs associated with the two rings. In DPM- d_0 , these modes are simple sums and differences of the two, and hence are delocalized over the two

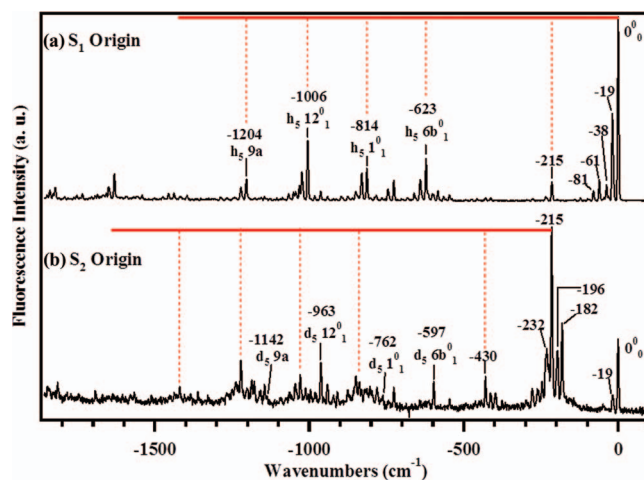


FIG. 5. DFL spectrum of the (a) S_1 origin and (b) S_2 origin. Prominent peaks are labeled by their assignment. Scattered light at the excitation wavelength was subtracted out.

TABLE II. Calculated and experimental ground state ring mode transitions for DPM- d_0 and DPM- d_5 and the degree of localization in DPM- d_5 .

Ring mode	DPM- d_0		DPM- d_5		Calculated localization
	Calc. ^a (cm ⁻¹)	Expt. (cm ⁻¹)	Calc. ^a (cm ⁻¹)	Expt. (cm ⁻¹)	
6a	567/626	554/610	561/600	...	Partially localized, mixed
6b	637/640	622	613/639	597/623	Localized
11	754/756	739	740/761	...	Delocalized, mixed
1	835/836	822	799/851	762/814	Partially localized, mixed
12	1022/1023	1006	980/1023	963/1006	Localized
9a	1212/1223	1204	1156/1218	1142/1204	Localized

^aCalculated at the B3LYP/cc-pVTZ level of theory.

rings. In DPM- d_5 , the degree of localization or delocalization can vary from one ring mode to the next, depending on the degree to which deuteration on one ring shifts its uncoupled frequency. Table II lists the ground state frequencies and degree of localization/delocalization of several of the ring modes that appear with reasonable Franck-Condon intensity in the dispersed fluorescence spectra of DPM- d_0 and DPM- d_5 . The assignments from Ref. 1 on DPM- d_0 show the degree to which the calculations correctly reproduce the experimentally observed splittings between the symmetric and antisymmetric combinations, which, with the exception of ν_{6a} , are no more than a few cm⁻¹. In DPM- d_5 , several of the ring mode pairs become quite highly localized on either the h_5 or d_5 ring, with a calculated frequency spacing between the two of 39 (ν_{6a}), 26 (ν_{6b}), 21 (ν_{11}), 52 (ν_1), 43 cm⁻¹ (ν_{12}), and 62 cm⁻¹ (ν_{9a}). As Figure 5 shows in DPM- d_5 a comparison of the ring-mode Franck-Condon activity shows a striking asymmetry in that the S_1 0^0 emission occurs preferentially to motion involving the h_5 ring rather than d_5 . This is a particularly intriguing point to which we will return in Sec. IV.

Figures 6(a)–6(g) show a close-up view of the first 200 cm⁻¹ of the DFL spectra for the S_1 origin and the vibronic bands built off of it. Given the near-complete assignments for the low frequency transitions in DPM- d_0 , it is possible to assign this low frequency structure. Furthermore, there is excellent agreement between the experimental ground state frequencies and the calculated values at the B3LYP/cc-pVTZ level that increase confidence in the assignments. As anticipated based on the LIF excitation spectrum, there are significant progressions in all the spectra in this series in the symmetric and antisymmetric torsional modes T and \bar{T} (Figures 6(b)–6(f)), with regular intervals of 19 and 16 cm⁻¹, respectively. Transitions assigned to T_n^0 with $n = 0-3$ and \bar{T}_0^m with $m = 0-2$ torsional modes could all be fit using a harmonic Franck-Condon analysis, with displacements D included in the figure caption. Furthermore, the S_1 origin DFL spectrum yields a transition at -61 cm⁻¹, which is assigned to the butterfly (β) mode fundamental. As Figure 6(g) shows, the transition at $+56$ cm⁻¹ in the excitation spectrum can be assigned as β_1^1 , in close agreement with its frequencies in DPM- d_0 .⁴

Figures 7(a)–7(e) present a series of DFL spectra from five weak transitions $+150$, $+191$, $+204$, $+213$, and $+225$ cm⁻¹ above the S_1 origin in the excitation spectrum of

Figure 2. The DFL spectrum of the $+150$ cm⁻¹ band (Figure 7(a)) displays a large false-origin band at -181 cm⁻¹, which can be assigned, based on the ground state calculations, to the \bar{R} fundamental (Figure 3(d)). By inference, then the transition in excitation is \bar{R}_0^1 . Similarly, the transition at $+191$ cm⁻¹ has a largest emission peak at -215 cm⁻¹ (Figure 7(b)), assignable as the R fundamental (Figure 3(c)). Both R and \bar{R} fundamentals have an antisymmetric \bar{T} combination built off

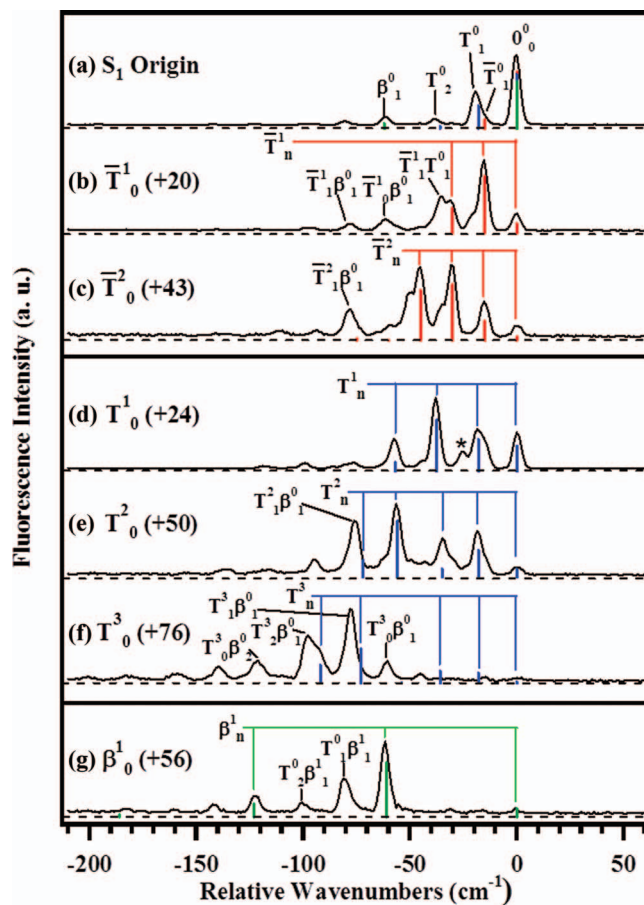


FIG. 6. DFL spectra from the (a) S_1 origin, (b) and (c) the antisymmetric torsion (\bar{T}) progression, (d)–(f) the symmetric torsion (T) progression, and (g) the butterfly (β) in DPM- d_5 . Prominent peaks are labeled by their assignment. The stick spectra correspond to FC simulations using (b) and (c) $D = 0.5$, (d)–(f) $D = 0.8$, and (g) $D = 0.5$. Scattered light at the excitation wavelength was subtracted out. The asterisk denotes the band ascribed to vibrational relaxation.

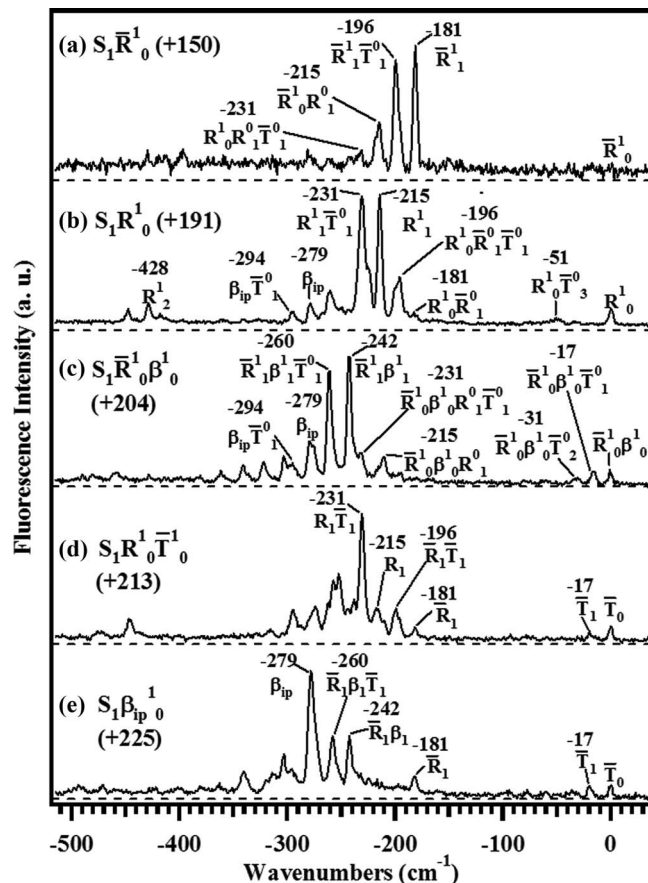


FIG. 7. DFL spectra of (a) \bar{R}_1^0 , (b) R_0^1 , (c) $\bar{R}_0^1\beta_0^1$, (d) $R_0^1\bar{T}_1^0$, and (e) β_{ip}^1 . Prominent peaks are labeled by their assignment. Scattered light at the excitation wavelength was subtracted out.

of them as well. Finally, Figure 7(c) (+204 cm^{-1}) shows the DFL spectrum of the $S_1 \bar{R}_0^1\beta_0^1$ transition, which also displays a largest emission peak in the corresponding $\Delta v = 0$ emission into the corresponding $\bar{R}_1\beta_1$ level at -242 cm^{-1} . The fact that these weak transitions in the excitation spectrum appear amidst several other bands of significantly greater intensity suggests that mixing with these nearby levels may occur.

Finally, the transitions at +213 and +225 cm^{-1} (Figures 7(d) and 7(e)) also have comparatively small S_2 character, with emission dominated by the $S_1(v)$ portion of the wave function. The emission in Figure 7(d) is dominated by a transition that ends in the $R_1\bar{T}_1$ ground state level, while that in Figure 7(e) lands at -279 cm^{-1} , a value very close to that calculated for the β_{ip} mode (280 cm^{-1}) shown in Figure 3(f). We thus tentatively assign the transitions in excitation at +213 and +225 cm^{-1} to $S_1 R_0^1 \bar{T}_1^0$ and $S_1 \beta_{ip}^1$, respectively, recognizing that all levels in this region are heavily mixed with one another.

2. S_2 origin and vibronic transitions

The overview DFL spectrum of the band assigned to the S_2 origin is shown in Figure 5(b), extending almost 2000 cm^{-1} to the red of its resonance fluorescence peak. Not surprisingly, this spectrum bears a distinct resemblance with the corresponding S_2 origin of DPM- d_0 itself.⁴ The spectrum is composed of two intermingled parts: the resonance

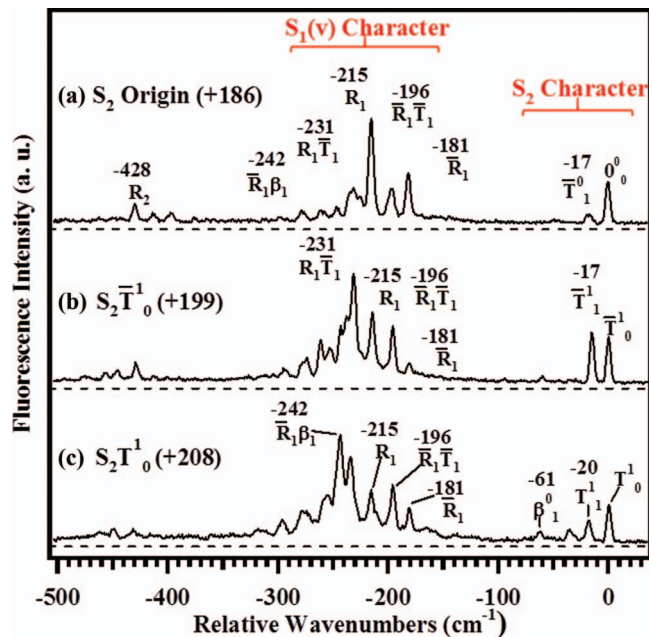


FIG. 8. DFL spectra from (a) the S_2 origin, (b) the antisymmetric torsion \bar{T}_1^0 , and (c) the symmetric torsion T_1^0 . Prominent peaks are labeled by their assignment. Scattered light at the excitation wavelength was subtracted out.

fluorescence and transitions built off it that are ascribed to the $S_2 0^0$ portion of the emission (connected by a tie-line in Figure 5(b)), and the so-called “clump emission” composed of the closely spaced set of transitions at -182 , -196 , -215 , and -232 cm^{-1} , and ring-mode activity built off of it. These transitions are shown in close-up view in Figure 8(a), with labels that reflect the ground state levels accessed by the emission. This emission is a characteristic signature⁴ of the set of close-lying $S_1(v)$ levels that are mixed with $S_2 0^0$ due to vibronic coupling between the two electronic states.

The +199 cm^{-1} transition in the excitation spectrum is assigned as $S_2 \bar{T}_1^0$ based on the DFL spectrum (Figure 8(b)), with intense transitions shifted up by one quantum in \bar{T} relative to those from the $S_2 0^0$. This indicates that the frequency of \bar{T} is only 13 cm^{-1} in the S_2 state (Table III), although its frequency position is likely to be shifted by the mixing. Based on the Franck-Condon activity involving the symmetric torsion T in the DFL spectrum of Figure 8(c), we assign the transition at +208 cm^{-1} to $S_2 T_1^0$, giving the symmetric torsion a frequency of 22 cm^{-1} in the S_2 state. Once again, the $S_2 T_1^0$

TABLE III. Experimental frequencies (cm^{-1}) of the vibrational modes for DPM- d_5 in the S_0 , S_1 , and S_2 electronic states.

Mode	Electronic state		
	S_0	S_1	S_2
T	19	24	22
\bar{T}	16	20	13
R	215	191	...
\bar{R}	181	150	...
β	61	56	...
β_{ip}	279	227	...

level is mixed with $S_1(v)$ levels that reveal themselves through the levels to which they emit with high probability. Given the known frequencies of \bar{R} (150 cm^{-1}) and β (56 cm^{-1}) in S_1 , the large emission to $\bar{R}_1\beta_1$ at -242 cm^{-1} is consistent with the close proximity of $\bar{R}_1\beta_1$ ($+206\text{ cm}^{-1}$) to the excitation frequency ($+208\text{ cm}^{-1}$).

IV. DISCUSSION

A. Vibronic coupling in DPM- d_5

It is interesting to compare the present results on DPM- d_5 to the symmetric case of DPM- d_0 in order to understand the implications for the vibronic coupling between the closely lying S_1 and S_2 states that result from deuteration of all hydrogens on one ring. In DPM- d_0 , the two UV chromophores are identical, and are in identical environments, leading to a pair of excited states that are, by symmetry, delocalized over the two rings, forming two excitonic states that can be viewed as sums and differences of the localized excitations on either ring: $\psi_{\pm} = \frac{1}{\sqrt{2}}(|X^*Y\rangle \pm |XY^*\rangle)$. In DPM- d_0 , the splitting between the S_1 and S_2 origins was 123 cm^{-1} . The DFL spectrum of the S_1 origin, when combined with an analysis of the transition dipole moment from the high resolution spectrum, confirmed that the S_1 zero-point level has its electronic excitation delocalized over both rings, much as the simple excitonic model would predict for this symmetric case.

Analysis of the DFL spectrum from the S_2 origin and $S_2 T^1_0$ transitions of DPM- d_0 showed, as in DPM- d_5 , that these upper levels are highly mixed with $S_1(v)$ levels in close proximity to them. Figure 9(a) reproduces a portion of the energy level diagram for DPM- d_0 from that earlier study.⁴ By symmetry, the $S_2 0^0$ and T^1 levels can only mix with $S_1(v)$ levels in which the vibrational symmetry is non-totally symmetric

(“b” symmetry in C_2). Beyond this symmetry restriction, the mixing with nearby levels was rather indiscriminate, mixing substantially with all levels in close energetic proximity, despite the fact that the changes in vibrational quantum numbers were large. For instance, the $S_2 0^0$ level mixed significantly with the $S_1 T^4\bar{T}^1$, $\bar{T}^3\beta^1$, $T^2\bar{T}^3$, and \bar{T}^5 levels (Figure 9(a)).

In DPM- d_5 , we have shown that the S_1 and S_2 origins are split by 186 cm^{-1} , nearly 50% larger than in DPM- d_0 . Zero-point energy differences between the two rings shift the uncoupled, zero-point levels of the two rings relative to one another. In some sense, the increased splitting might be thought of as a site splitting, but we intentionally avoid this language in what follows, because the S_1 origin has a TDM direction that is nearly identical to that in DPM- d_0 , and its electronic excitation is therefore delocalized over the two rings, much as it is in DPM- d_0 .

Figure 9(b) contrasts the energy level mixing diagram in the region of the S_2 origin for DPM- d_5 with that in DPM- d_0 . The diagram highlights that, upon deuteration of one ring, symmetry restrictions on the vibrational levels and internal mixing between them are removed. In this figure, we have not included the full set of $S_1(v)$ levels in the diagram, but only that subset that is involved significantly in the S_1/S_2 mixing. Note first that the energy splitting between S_1 and S_2 states induced by deuteration is now 186 cm^{-1} . If all low frequency torsional and bending levels were included in the diagram, it would be significantly more complex, with an S_1 vibrational density of states at 186 cm^{-1} of 2 states/ cm^{-1} . In this respect, the internal mixing in DPM- d_5 involves a rather small subset of levels that reach over somewhat greater energy spread than in DPM- d_0 itself. In the diagram in Figure 9(b), the levels involved in the mixing are connected by lines whose widths reflect the magnitude of the mixing. The dominant mixing is shown in each case with a double-headed arrow.

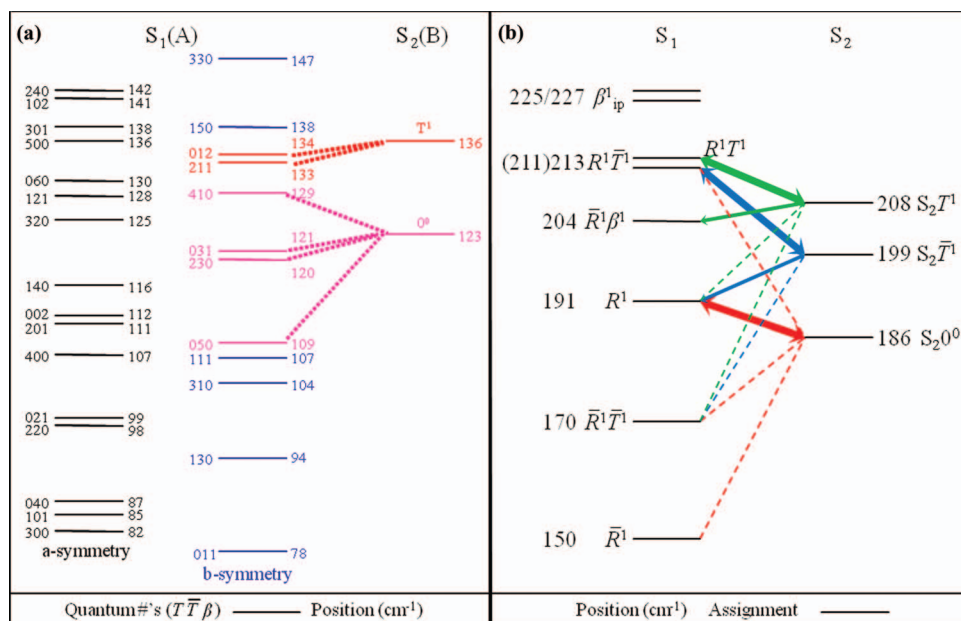


FIG. 9. Comparison between the energy levels and mixing in (a) DPM- d_0 with (b) DPM- d_5 . Each energy level of DPM- d_0 is designated with a set of quantum numbers ($T \bar{T} \beta$) and a wavenumber position (in cm^{-1}), while only the subset of levels involved in the mixing is shown for DPM- d_5 . The coupled levels are connected by double-headed arrows (principle coupling) and dotted lines (secondary).

This leads to a remarkably simple picture. The S_2 0^0 level, 186 cm^{-1} above its S_1 counterpart, is in close proximity to S_1 R^1 (191 cm^{-1}), and serves as the dominant level involved in the internal mixing. In DPM- d_0 , this mixing was zero by symmetry, but here it is allowed. Furthermore, the larger splitting between S_1 and S_2 states has moved S_2 0^0 into near resonance with S_1 R^1 , and therefore makes possible internal mixing involving the usual $\Delta v = 1$ Herzberg-Teller (HT) coupling. Furthermore, the second-most intense emission band is at -181 cm^{-1} , assigned to \bar{R}_1 , even though the S_1 \bar{R}^1 level is 36 cm^{-1} below S_2 0^0 . Thus, the $\Delta v = 1$ HT selection rules dominate over mixing with a host of other levels with larger Δv that are much closer in energy.

Similarly, as Figure 9(b) summarizes, the (nominal) S_2 \bar{T}^1 and S_2 T^1 levels also are prominently engaged in mixing with $S_1(v)$ levels with $\Delta v_R = 1$. Only in the latter case is a level that violates $\Delta v = 1$ mixed with similar strength, involving the S_1 $\bar{R}^1\beta^1$ level that is only 5 cm^{-1} away from S_2 T^1 . Thus, whenever possible, near-degenerate mixing is dominated by $\Delta v = 1$ selection rules. In DPM- d_5 , mode R is of a frequency to bridge the gap between the two electronic states, and therefore dominates the mixing.

At the same time, higher-order HT mixing is certainly also at play, and clearly observable as a mechanism for secondary mixing (dashed lines in Figure 9(b)). Indeed, a more complete description of the excited state vibronic character of the (nominal) S_2 origin is

$$|+186\text{ cm}^{-1}\rangle = c_1|S_2, 0^0\rangle + c_2|S_1, R^1\rangle + c_3|S_1, R^1\bar{T}^1\rangle + c_4|S_1, \bar{R}^1\rangle + c_5|S_1, \bar{R}^1\bar{T}^1\rangle + \dots, \quad (1)$$

where we have listed the five largest contributions to the wave function based on the intensities of the emission to the ground state levels. Note that, while the $\Delta v = 1$ HT selection rules do not hold for terms 3 and 5 in Eq. (1), they nevertheless all involve Δv_{tot} which are quite small, as might be anticipated if the coupling strength falls off in size with each increase in Δv_{tot} .

The qualitative picture just presented for vibronic coupling in DPM- d_5 , while pleasing in its own right, also calls for a deeper, and more quantitatively accurate description. For instance, the present analysis has not addressed explicitly vibronic coupling involving the Franck-Condon active ring modes, which are known to be of primary importance for S_1/S_2 mixing, and would add further terms to the wave function beyond those shown in Eq. (1). This deeper analysis is left for the theoretical modeling described in Ref. 7.

B. Molecular structural analysis of DPM- d_5 from high resolution UV spectroscopy

We now shift attention to the implications of the internal mixing for the rotational structure present in the rotationally resolved spectra presented in Sec. III B. Beyond the reduction in symmetry associated with deuterium substitution on one of the rings of DPM- d_0 , this substitution also increases the mass of one ring, and therefore should cause some rotation of the principal inertial axis frame (PAF). Indeed, in the ground

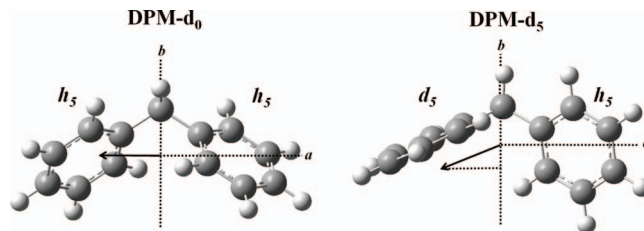


FIG. 10. (a) S_1 TDM orientation of DPM- d_0 for the (α, τ) fit structure and (b) S_1 TDM orientation transformed into the frame of DPM- d_5 . The S_1 TDM of DPM- d_0 has both a -type and a c -type component (not shown) which upon rotation into the frame of DPM- d_5 gives 11% b -type character (see text for details).

state, this slight rotation enabled the observation of some c -type transitions in the microwave (MW) spectrum. However, the large uncertainties in the measured amplitudes of the b - and c -type transitions preclude any quantitative assessment of the degree of inertial frame rotation.

On the other hand, the ground state MW rotational constants are well-determined and with the aid of *ab initio* theory, the orientation of the PAF in DPM- d_5 relative to the C_2 symmetry axis of DPM- d_0 may be estimated by a method similar to that discussed previously.⁵ Beginning with the optimized structure of DPM- d_0 at the MP2/cc-pVTZ level (shown in Figure 10), two structural parameters, τ and α , were least squares fit to the three experimental moments of inertia, where the dihedral angle, τ , defines the symmetric torsional motion of the two rings and α defines the CCC angle between the rings. From the results given in Table IV, the fits reduce the difference in the theoretical versus observed rotational constants by more than two orders of magnitude to 0.1 MHz or less. The best fit values for τ and α are 57.6° and 114.6° , respectively and are very similar to the values of 58.2° and 114.6° fit to the observed inertial moments of DPM- d_0 .⁵ Also given in Table IV are the results of fitting the dihedral angles, τ_1 and τ_2 , of the d_5 and h_5 rings independently. In this case, the difference in the angles, τ_1 and τ_2 , is only 0.3° . In either case, the reorientation of PAF relative to DPM- d_0 is primarily a small rotation about the a -inertial axis.

C. Transition dipole moment orientation analysis of DPM- d_5

The TDM orientations obtained from the rotationally resolved UV spectra have been used in previous studies of the C_2 symmetric structures of DPM- d_0 , DPM- d_{12} , and b4HPM to establish the delocalized nature of both S_1 and S_2 electronic states of these systems.^{5,23} For DPM- d_0 and DPM- d_{12} , the S_1 states were found to be hybrid bands containing only a - and c -type rotational transitions with component magnitudes in the ratio of 65(2)%:35(2)% and 67(2)%:33(2)%, respectively. The TDM orientations are perpendicular to the C_2 symmetry axes of these systems and indicate an anti-symmetric combination of localized electronic wave functions on each of the chromophores. The S_2 states, although not fit, were found to have rotational structure characteristic of pure b -type rotational bands as expected for TDM

TABLE IV. The experiment and calculated structural parameters of DPM- d_5 are given using the MP2/cc-pVTZ optimized structure. The *ab initio* structure was fit to the observed moments of inertia by varying the angle, α , between the rings and the ring dihedral angles, τ , together and independently using τ_1 , τ_2 .

Parameter	Expt. ^a	Opt	Fit ^b	E-F ^c	Parameter	Opt	Fit ^b	E-F ^c
A'' (MHz)	1884	1842	1884	0.0	A'' (MHz)	1842	1884	0.0
B'' (MHz) ^d	404.6	414.7	405	-0.1	B'' (MHz) ^d	414.7	405	0.0
C'' (MHz)	399.5	409.5	400	-0.1	C'' (MHz)	409.5	400	0.0
A (deg)		111.9	115	-2.7	α (deg)	111.9	115	-2.7
τ (deg)		58.7	57.6	+1.1	τ_1 (deg)	58.7	57.4	+1.3
					τ_2 (deg)	58.7	57.7	+1.0

^aExperimental rotational constants obtained from MW measurements and rounded for clarity.

^bThe fits were weighted according to the inertial uncertainties propagated from the rotational constants.

^cExperimental fit values for the rotational constants and optimized (Opt) minus fit values for α and τ .

^dAxis designates the C_2 symmetry axis.

orientations parallel to the C_2 symmetry axes. In a later study of two symmetric conformers of *b*4HPM,²³ the S_1 and S_2 excitonic states were fully fit, confirming the delocalized nature of the electronic wave functions of these systems. In this section, we make use of the observed TDM orientation (Table I) and the fitted geometries of DPM- d_5 (Table IV) to examine whether the nuclear asymmetry resulting from deuterium substitution leaves the delocalized nature of the excitonic states in tact or changes it to localized excitation on each of the rings.

Making use of the fitted geometries in Sec. IV B, the inertial axis reorientation of the PAF may be used to determine the S_1 TDM components of DPM- d_0 in the frame of DPM- d_5 . To apply this transformation, the principal axis coordinates of the two fitted geometries are first determined assuming a d_0 -structure. The TDM vector of the delocalized S_1 state that gives the observed *a:c*-type ratio of 65%:35% is then transformed into the PAF of DPM- d_5 by diagonalization of the inertial tensor. While no ambiguity exists from the fits as to which ring is d_5 , the signed direction of the TDM vector in DPM- d_0 becomes important in the transformation (these signs are not determined from the band type intensities). Four sign combinations are possible with a two component TDM vector that describes the S_1 state of which only two are unique. Using the (τ, α) geometry, the transformed compositions of the two are similar and give 66%:11%:23% which over-predicts the *b*-type observed intensity by 8%. For the (τ_1, τ_2, α) geometry where τ_1 and τ_2 are fit independently, the predicted TDM components in the PAF frame of DPM- d_5 are 66%:4%:30% and 66%:5%:29%. Both ratios are in good agreement with the experimental S_1 ratio of 66(2)%:3(1)%:31(2)%. From these results, it is clear that small changes in the relative orientation of the two rings impact on the observed TDM orientation principally through rotation about the *a*-axis. It is also clear that the small *b*-type component of the S_1 state can be largely explained based on the inertial axis rotation about the *a*-axis and like that of DPM- d_0 suggests the S_1 electronic state is delocalized despite the nuclear asymmetry. In sharp contrast, applying this same transformation to the pure *b*-type TDM of the S_2 state of DPM- d_0 , the model predicts 0%:67%:33% for the (τ, α) geometry and 0%:87%:13% for the (τ_1, τ_2, α) geometry. In either case, the large *a*-type intensity observed in the S_2 state fit is not reproduced.

One limiting case to consider would be where complete electronic localization occurs, leading to excited state wave functions for the $-h_5$ and $--d_5$ rings that are uncoupled and excited independently. For a description of localized electronic states of DPM- d_0 , the observed components of the TDMs would be the PAF projections of μ_{local} of each ring which are given by the sum and difference of the observed delocalized orientations of the S_1 and S_2 states. This gives μ_{local} on each ring having an intensity ratio of 55%:17%:28% (after renormalization) This model assumes that vibronic coupling that leads to state mixing in DPM- d_0 is "switched off" in DPM- d_5 because of the nuclear asymmetry, a point to which we return below. For a three component TDM vector of DPM- d_0 , eight possible sign combinations are possible of which only four are unique as discussed in Ref. 2. Furthermore, of the four, only two pairs of the solutions differ by more than 1%. Transformation of the localized TDM vectors into the frame of DPM- d_5 gives 55%:0%:45% and 56%:40%:4% for the (τ, α) geometry and 54%:4%:41% and 56%:32%:12% for the (τ_1, τ_2, α) geometry. The principal axis orientations for the (τ, α) geometry are shown in Figure 10 for the DPM- d_0 and DPM- d_5 geometries. While significant *a*-type components exist in these ratios for both the S_1 and S_2 states of DPM- d_5 , none of them explains the well-determined S_1 components of 66(2)%:3(1)%:31(2)% or are within the much larger uncertainties of the S_2 components of 30(10)%:50(10)%:20(10)%.

Instead, the experimental data indicate that the S_1 state remains delocalized in DPM- d_5 , leading to the postulate that the odd appearance of significant *a*-type character in the S_2 origin has its origin in vibronically induced state mixing of the S_1 and S_2 states that is present already at the S_2 zero-point level. Indeed, the vibronic coupling modeling, which will be discussed in detail in Ref. 7, predicts 71%:4%:25% composition for S_1 and 19%:74%:7% composition for the S_2 origin. These predictions are in line with the rotationally fitted TDM components. Especially encouraging is a significant *a*-type character determined by the vibronic model for the S_2 origin, which strongly supports the state-to-state picture of internal mixing addressed by the model. What must be addressed yet are other aspects of the vibronic spectroscopy, most notably the observed Franck-Condon activity of torsional and ring modes, which suggest electronic localization even in S_1 levels where this is known not to be the case.

D. Vibrational and electronic energy localization in DPM- d_5

While in some ways the effects of deuteration of one ring on the spectroscopy and excited state vibronic mixing in DPM- d_5 are rather modest, in other ways they are strikingly obvious, and a bit puzzling. As already pointed out, the appearance of such a strong S_0 - S_1 \bar{T}_0^1 fundamental in the DPM- d_5 excitation spectrum (Figure 2) is in striking contrast to its forbidden nature in DPM- d_0 , even more so because the high resolution UV spectrum has proven that electronic excitation in S_1 is still delocalized over both rings in DPM- d_5 . Furthermore, the S_1 origin DFL spectrum (Figure 5(a)) has Franck-Condon activity involving three highly localized ring modes (6b, 12, 9a) that shows a strong asymmetry, in that emission to the ground state vibrational levels involving motion of the $-h_5$ ring is much larger than the corresponding emission to its $-d_5$ ring counterparts. Likewise, the S_2 origin DFL spectrum shows emission involving the same ring modes from the S_2 0^0 portion of the excited state wave function favoring the $-d_5$ ring modes.

As we will show in the theoretical paper,⁷ one of the triumphs of the vibronic coupling model developed there is its

ability to reproduce these asymmetries in quantitative fashion. While a description of the detailed model is left for that work,⁷ we present here a physical picture that provides a qualitative explanation of these experimental anomalies.

Localization of the vibrational wave functions occurs due to several effects produced by the asymmetric deuteration of the monomers. The first effect, reproduced by the electronic structure calculations, is the localization of the 6b, 12, and 9a vibrations to the individual aromatic rings. Due to the weak kinematic coupling between the two chromophores in all electronic states, the small mass perturbation causes a rotation of the nuclear wave functions from symmetric/antisymmetric pairs to vibrations localized on individual monomers.

Once the vibrations are localized, an examination of the electronic Hamiltonian reveals that the geometry at which the electronic excitation is perfectly delocalized is no longer the geometry at which both vibrations are displaced from their equilibrium positions by equal amounts. Working in the diabatic electronic basis, the system Hamiltonian can be written (considering only one vibration on each monomer):

$$\begin{bmatrix} \hbar\omega_H(Q_H + Q_0)^2 + \hbar\omega_D(Q_D)^2 & V \\ V & \hbar\omega_H(Q_H)^2 + \hbar\omega_D(Q_D + Q_0)^2 \end{bmatrix}. \quad (2)$$

Here Q is a vibrational coordinate for either the deuterated or non-deuterated ring (labeled accordingly), ω is the corresponding localized vibrational frequency, Q_0 is the displacement along a normal mode upon electronic excitation of the corresponding chromophore, and V is an electronic coupling constant. The electronic states become completely delocalized in this model Hamiltonian when the two diagonal elements become equal. However, since $\omega_H > \omega_D$ due to the isotope effect, the electronic states become perfectly mixed when $Q_D > Q_H$ (assuming $Q_0 > 0$). This effect can be observed in the S_1 state potential energy surface in Figure 11. In this figure the color of the surface indicates whether the electronic excitation prefers to localize on the d_5 -ring (orange) or the h_5 -ring (blue). In Figure 11(a) the parameters are completely symmetric and thus the change from orange to blue happens along $Q_a = Q_b$, while in Figure 11(b) the change happens when $Q_D > Q_H$.

An additional contribution to the localization of the vibrational Franck-Condon activity of the S_1 state on the h_5 -ring arises due to differences in zero point energies (ZPEs) of the vibrations not directly included in the vibronic coupling Hamiltonian. Vibrational frequencies in the excited state are on average smaller than those in the ground state due to the reduced bonding character of the excited state. If this reduction in frequency affects both the h_5 - and d_5 -rings by the same multiplicative factor, the difference in ZPEs between the

ground and excited states will cause the diabatic state in which the h_5 -ring is excited to be slightly lower in energy than the state in which the d_5 -ring is excited. This change in ZPEs can be represented by adding a small energy (approximately an order of magnitude less than the frequency values) to the lower right Hamiltonian element. The effect of this parameter can be observed in Figure 11(b) by noting that the well with $Q_D < 0$ (right side of PES) is shallower than the well with $Q_H < 0$ (left side of PES). This slight asymmetry in the depth of the two wells causes the S_1 state to localize around $Q_H = -Q_0$ and $Q_D = 0$. However, as noted above, this is nearly precisely where the two electronic states are completely

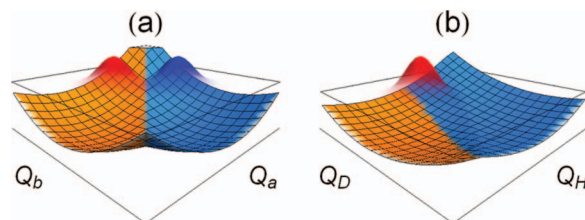


FIG. 11. The potential energy surface (solid) and wave function (transparent) for two localized vibrations with symmetric parameters (frame (a)), and asymmetric parameters representing a partially deuterated bichromophore (frame (b)). The color of the surface indicates which monomer the excitation prefers to localize on, with blue representing the a/h_5 -ring and orange representing the b/d_5 -ring. Further explanation can be found in the text.

mixed from the Hamiltonian in Eq. (2). As a result, both the localization of the h_5 -ring Frank-Condon activity on the S_1 state and the delocalization of the S_1 electronic state take place. A more complete and quantitative explanation of this intriguing observation will be given in Ref. 7.

V. CONCLUSIONS

This detailed study of vibronic coupling, or internal mixing as it is sometimes called, in DPM- d_5 , constitutes a first important step in developing a model for this mixing in asymmetric bichromophores. The simple act of deuteration of one rings has shifted the spacing between S_1 and S_2 states to 186 cm^{-1} , an amount sufficient to bring each $S_2(v)$ level into close proximity with $S_1(v, R^1)$, since $\nu_R(S_1) = 191\text{ cm}^{-1}$. This near-resonance with a level that can engage with it in Herzberg-Teller allowed $\Delta\nu_R = 1$ coupling is shown clearly in the DFL spectra, dominating the $\Delta v = 0$ emission from $S_1(v)$ levels involved in this mixing. By contrast, in the symmetric counterpart, DPM- d_0 , the energy splitting is 123 cm^{-1} , an amount that places the S_2 zero-point level in an energy gap without S_1 vibrational fundamentals of the right symmetry and frequency, leaving only levels with larger Δv in close proximity, which then take up a role as the principle means for near-resonant mixing. The nominal S_2 origin also shows its mixed $S_2/S_1(v)$ character through its TDM orientation, which is no longer perpendicular to that of the S_1 origin.

The emission from $S_1\ 0^0$ and $S_2\ 0^0$ to the ring modes showed evidence of vibronic coupling that was decidedly counter-intuitive. There, the S_1 emission occurred preferentially to ring modes whose nuclear motion was localized primarily on the $-h_5$ ring, while the S_2 emission occurred to levels involving the $-d_5$ ring. A model that builds and diagonalizes electronic-vibrational Hamiltonian based on parameters from *ab initio* calculations was used to qualitatively explain localization/delocalization patterns in vibronic states. This model provides a framework to interpret mode pairs present in other bichromophores in which the two chromophores are chemically similar, and thus have ring modes that are similar to one another in form and frequency. The physical insight provided by the model into internal mixing shows promise for its application to a wider range of asymmetric bichromophores. Among the targets for future work include 1,1-

diphenylethane and 1,1-diphenylpropane, in which the degree of asymmetry increases with increasing alkyl chain length.

ACKNOWLEDGMENTS

N.R.P., N.M.K., and T.S.Z. gratefully acknowledge that this material is based upon work supported by the U.S. Department of Energy Office of Science, Office of Basic Energy Sciences under Award No. DE-FG02-96ER14656. B.N. and L.V.S. acknowledge support from the National Science Foundation Career Grant No. CHE-0955419 and Purdue Research Foundation.

- ¹A. Muller, F. Talbot, and S. Leutwyler, *J. Chem. Phys.* **116**, 2836 (2002).
- ²N. A. van Dantzig *et al.*, *J. Chem. Phys.* **103**, 4894 (1995).
- ³A. Zehnacker *et al.*, *Chem. Phys.* **208**, 243 (1996).
- ⁴N. R. Pillsbury *et al.*, *J. Chem. Phys.* **129**, 114301 (2008).
- ⁵J. A. Stearns *et al.*, *J. Chem. Phys.* **129**, 224305 (2008).
- ⁶B. Nebgen, F. L. Emmert, and L. V. Slipchenko, *J. Chem. Phys.* **137**, 084112 (2012).
- ⁷B. Nebgen and L. V. Slipchenko, "Vibronic coupling in asymmetric bichromophores: Theory and application to diphenylmethane- d_5 ," *J. Chem. Phys.* (submitted).
- ⁸J. P. Finley and J. R. Cable, *J. Phys. Chem.* **97**, 4595 (1993).
- ⁹F. A. Ensminger *et al.*, *J. Chem. Phys.* **102**, 5246 (1995).
- ¹⁰See supplementary material at <http://dx.doi.org/10.1063/1.4892344> for details of the synthesis of DPM- d_5 , rotational constants, and distortion parameters from least squares fits of the ground state and $S_1 \leftarrow S_0$ spectra, assigned lines in the ground state microwave spectrum, and rotationally resolved UV spectra of select vibronic bands.
- ¹¹D. F. Plusquellic, S. R. Davis, and F. Jahanmir, *J. Chem. Phys.* **115**, 225 (2001).
- ¹²W. Majewski and W. L. Meerts, *J. Mol. Spectrosc.* **104**, 271 (1984).
- ¹³D. F. Plusquellic *et al.*, *Chem. Phys.* **283**, 355 (2002).
- ¹⁴E. Riedle *et al.*, *Rev. Sci. Instrum.* **65**, 42 (1994).
- ¹⁵R. D. Suenram *et al.*, *Rev. Sci. Instrum.* **70**, 2127 (1999).
- ¹⁶M. J. Frisch, G. W. Trucks, H. B. Schlegel *et al.*, Gaussian 09, Gaussian, Inc., Wallingford, CT, 2009.
- ¹⁷W. L. Meerts, M. Schmitt, and G. C. Groenenboom, *Can. J. Chem.* **82**, 804 (2004).
- ¹⁸D. F. Plusquellic *et al.*, *J. Chem. Phys.* **115**, 3057 (2001).
- ¹⁹D. F. Plusquellic, JB95 Spectral fitting program, v2.07.08, National Institute of Standards and Technology, 2009.
- ²⁰P. E. Gordon and A. J. Fry, *Tetrahedron Lett.* **42**, 831 (2001).
- ²¹J. B. Hopkins, D. E. Powers, and R. E. Smalley, *J. Chem. Phys.* **72**, 5039 (1980).
- ²²B. N. Taylor and C. E. Kuyatt, NIST Technical Note 1297, 1994, see <http://physics.nist.gov/Pubs/guidelines/contents.html>.
- ²³C. P. Rodrigo *et al.*, *J. Chem. Phys.* **134**, 164312 (2011).